Efficient Quasi-Classical Trajectory Calculations by means of Neural Operator Architectures

Maitreyee Sharma Priyadarshini,[1] Simone Venturi,[1] Ivan Zanardi,[1] and Marco Panesi[1, a)]

Center for Hypersonics & Entry Systems Studies, Department of Aerospace Engineering,

University of Illinois, Urbana-Champaign, Urbana, Illinois 61801,
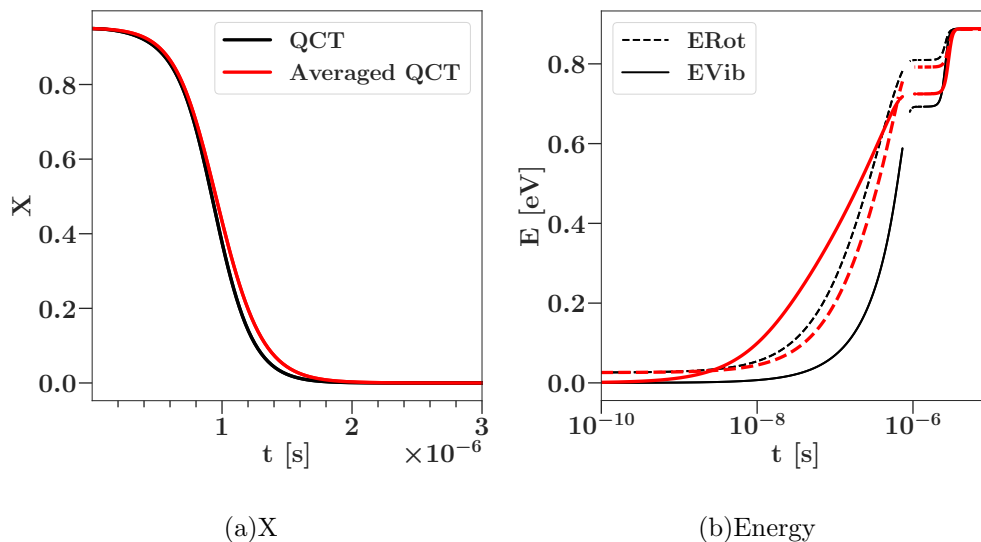
USA

(Dated: May 8, 2023)

---

a)Electronic mail: mpanesi@illinois.edu

CONTENTS

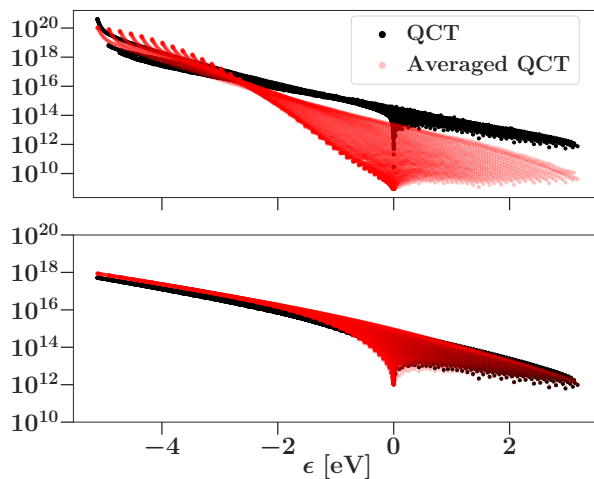# I. RESULTS OBTAINED FROM AVERAGED STS RATE COEFFICIENTS

(a)X

(b)Energy

(c)Population Distribution at t = 1e-7 s (top) and

quasi-steady state (bottom)

Figure S1: Solutions of the master equation for the O_2+O system. The results in black are obtained using QCT state-to-state (StS) rate coefficients. The results in red, instead, are produced by applying $(v \pm 2, J \pm 2)$ window-averaging over the same QCT database before running the master equation, as proposed by Koner *et al.* (*i.e.*, Eq. 1 of reference[1]). Comparisons are made for the (a) mole fraction, (b) evolution of rotational and vibrational energies, and (c) population distributions at two time-instants. All the results are obtained by considering a translational temperature T = 10,000 K.

II. RATE PATTERNS
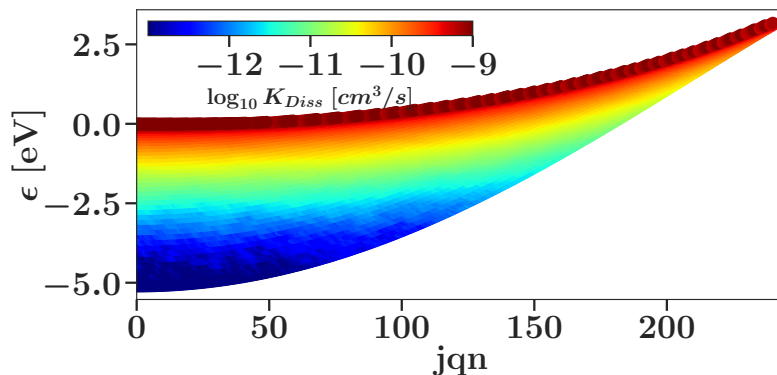

Figure S2: Patterns observed in StS reaction rate coefficients for dissociation processes. While we only report the results at T = 10,000 K, similar patterns have also been observed at all the other analyzed temperatures.
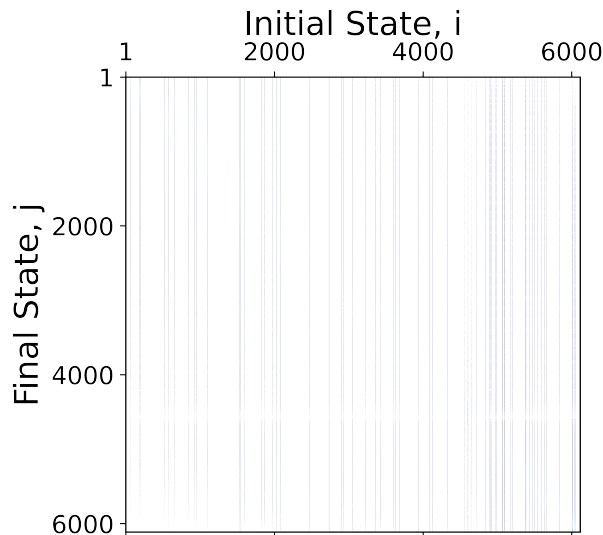

Figure S3: The 90 columns of the T = 20,000 K state-to-state reaction rate coefficient matrix used to train the SurQCT surrogate for the O_2+O inelastic processes. Four additional matrices with only 90 non-zero columns each are also included as training data, corresponding to coefficients at T = 1,500, 5,000, 10,000, 15,000 K. The figure aims to show the relative sparsity of the training data compared to the original rate coefficient matrices.

III.   ARCHITECTURES OF THE THREE SURROGATE COMPONENTS
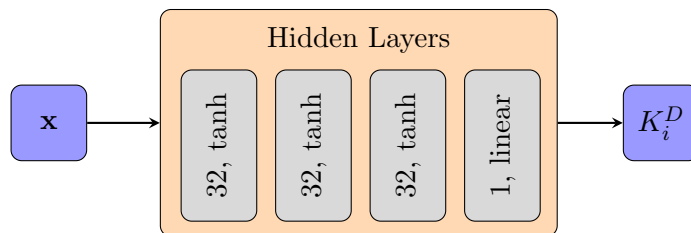
Figure S4: Feed-forward neural network (FNN) architecture used for dissociation reaction rates surrogation. The input vector is: $\mathbf{x} = [\Delta E_{CB}, \log_{10}(r_{max}), \log_{10}(r_o), T]^{\mathrm{T}}$. A dropout layer with a rate of 10^{-3} is applied at the end of each hidden layer, excluding the last one. L1 and L2 regularization parameters are set to 10^{-4} and 10^{-5}, respectively.
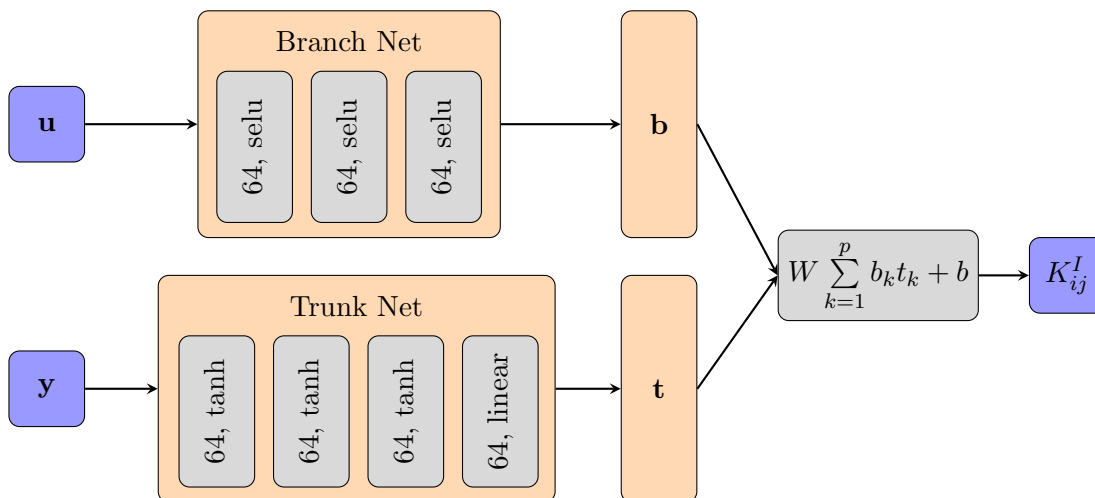
Figure S5: Unstacked deep operator network (DeepONet) architecture used for inelastic reaction rate coefficients surrogation. The inputs to the branch are: $\mathbf{u} = [\log_{10}(\epsilon_{Vib}), \log_{10}(\epsilon_{Rot}), \log_{10}(r_o), T]^{\mathrm{T}}$ and to the trunk are: $\mathbf{y} = [\Delta \log_{10}(\epsilon_{Vib}), \Delta \log_{10}(\epsilon_{Rot}), \Delta \log_{10}(r_o), T]^{\mathrm{T}}$. A dropout layer with a rate of 10^{-2} is applied at the end of each hidden layer, excluding the last one. L1 and L2 regularization parameters are set to 10^{-5} and 10^{-5}, respectively.
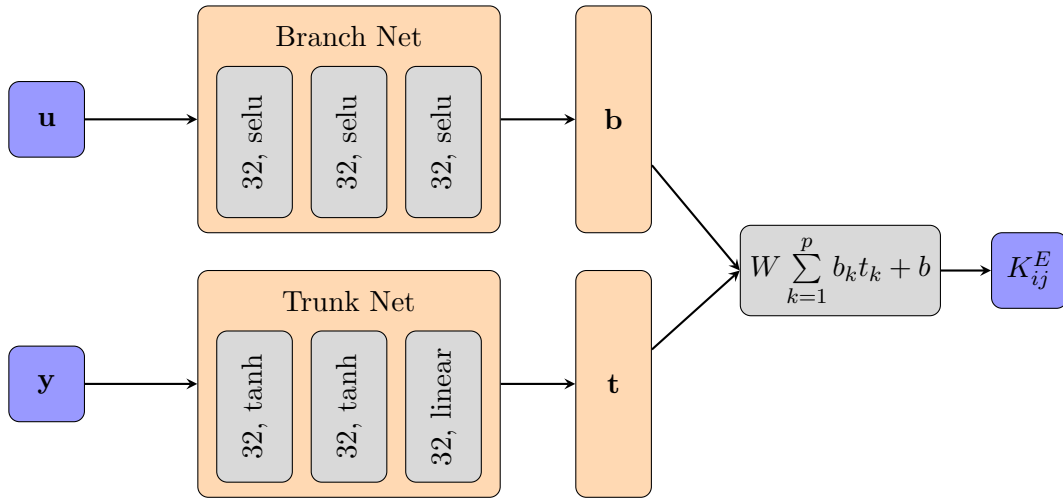
Figure S6: Unstacked deep operator network (DeepONet) architecture used for inelastic reaction rate coefficients surrogation. The inputs to the branch are: $\mathbf{u} = [\log_{10}(\epsilon_{Vib}), \log_{10}(\epsilon_{Rot}), \log_{10}(r_o), T]^{\mathrm{T}}$ and to the trunk are: $\mathbf{y} = [\Delta \log_{10}(\epsilon_{Vib}), \Delta \log_{10}(\epsilon_{Rot}), \Delta \log_{10}(r_o), T]^{\mathrm{T}}$. A dropout layer with a rate of 10^{-3} is applied at the end of each hidden layer, excluding the last one. L1 and L2 regularization parameters are set to 10^{-4} and 10^{-4}, respectively.

IV. WEIGHTING SCHEME FOR THE NEURAL NETWORK LOSS FUNCTION

| Rate Coefficients Value	Weight
$K > 10^{-9}$	15.0
$10^{-10} < K \leq 10^{-9}$	12.0
$10^{-11} < K \leq 10^{-10}$	9.0
$10^{-12} < K \leq 10^{-11}$	6.0
$10^{-13} < K \leq 10^{-12}$	3.0
$K \leq 10^{-13}$	1.0

Table I: Weighting scheme for the loss function based on the magnitude of the reaction rate coefficients for all collisional processes.

V. QUALITY OF SURQCT PREDICTIONS FOR THE REACTION RATE COEFFICIENTS
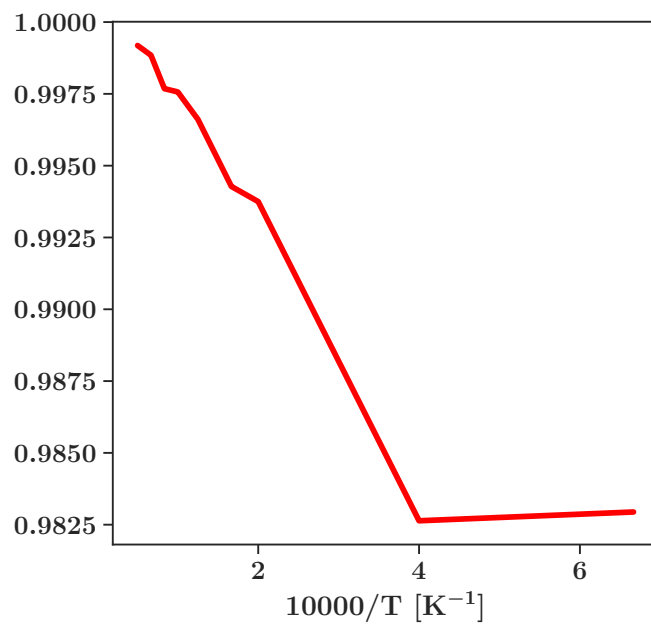
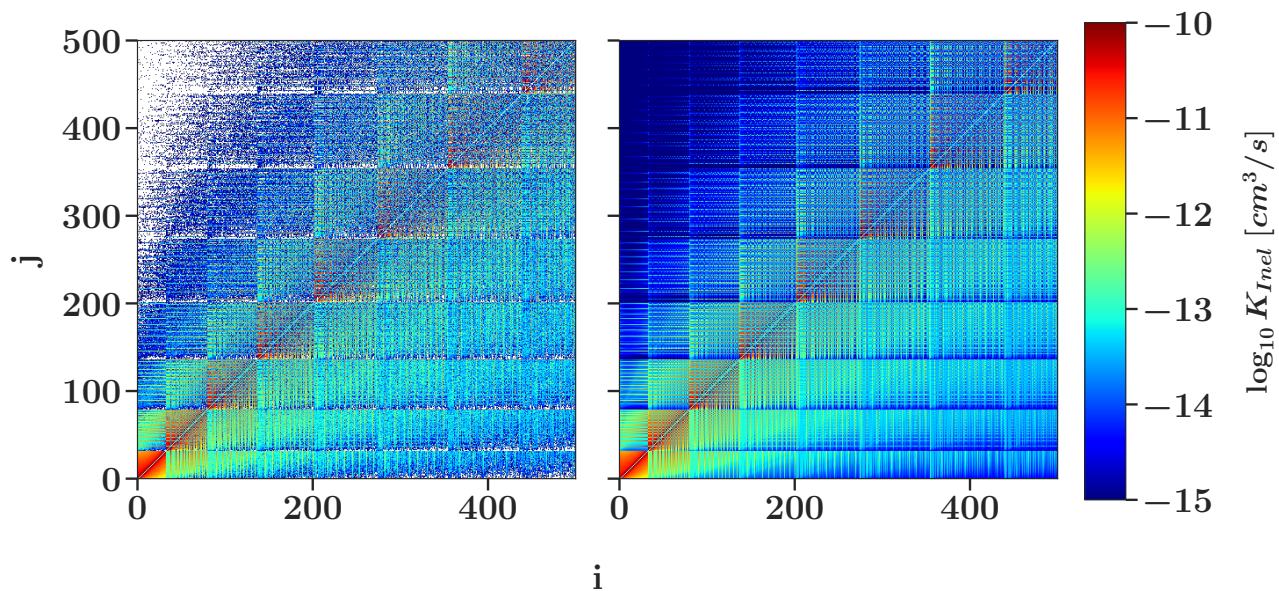

Figure S7: R^2 values for the SurQCT predictions computed with respect to the reference QCT dissociation reaction rate coefficients.
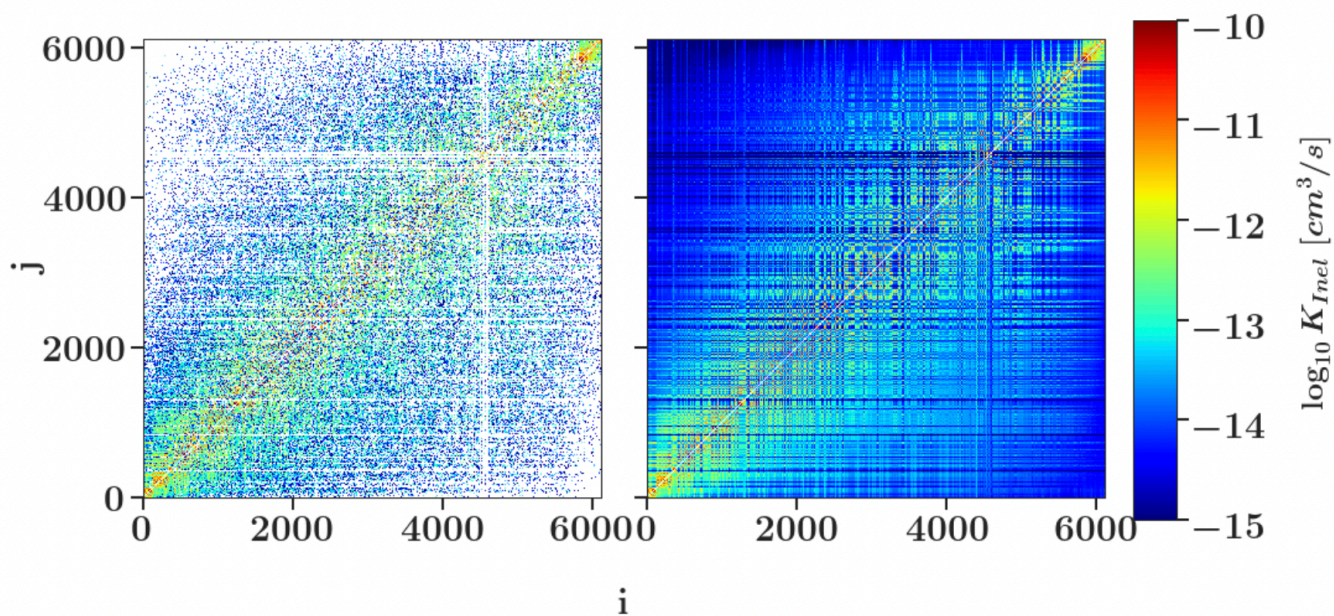
VI.   INELASTIC AND EXCHANGE REACTION RATE COEFFICIENTS
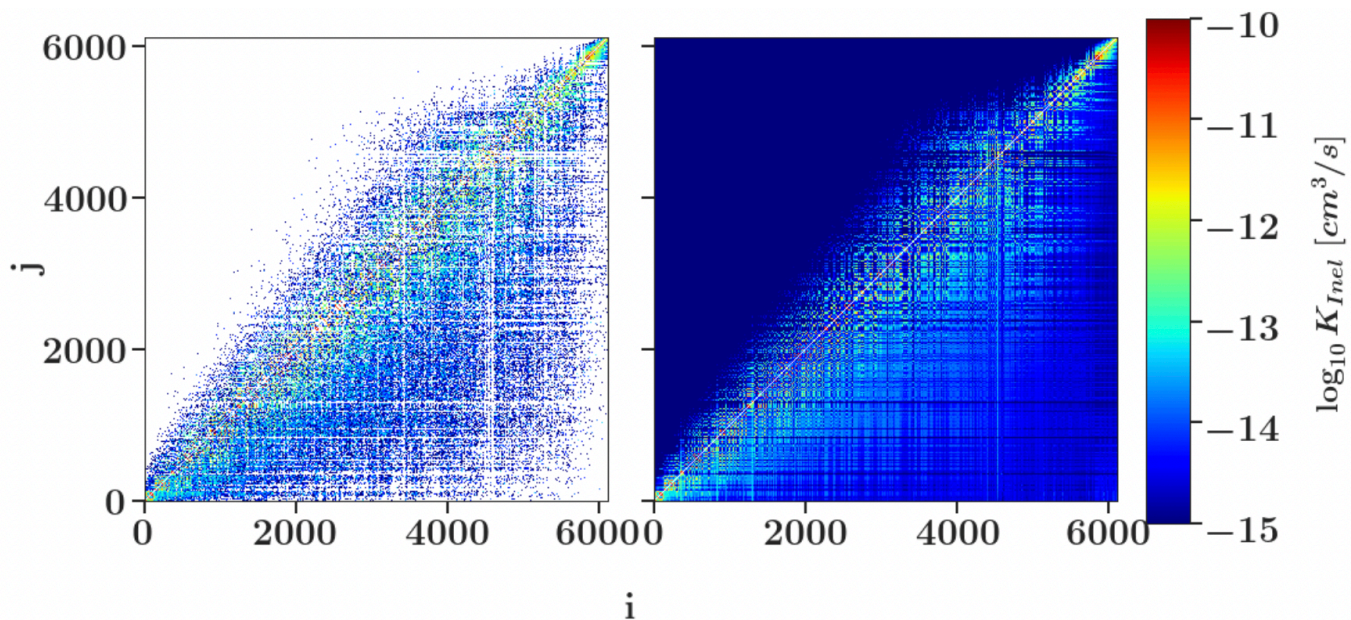
(a)Full StS Inelastic Rate Coefficient Matrix

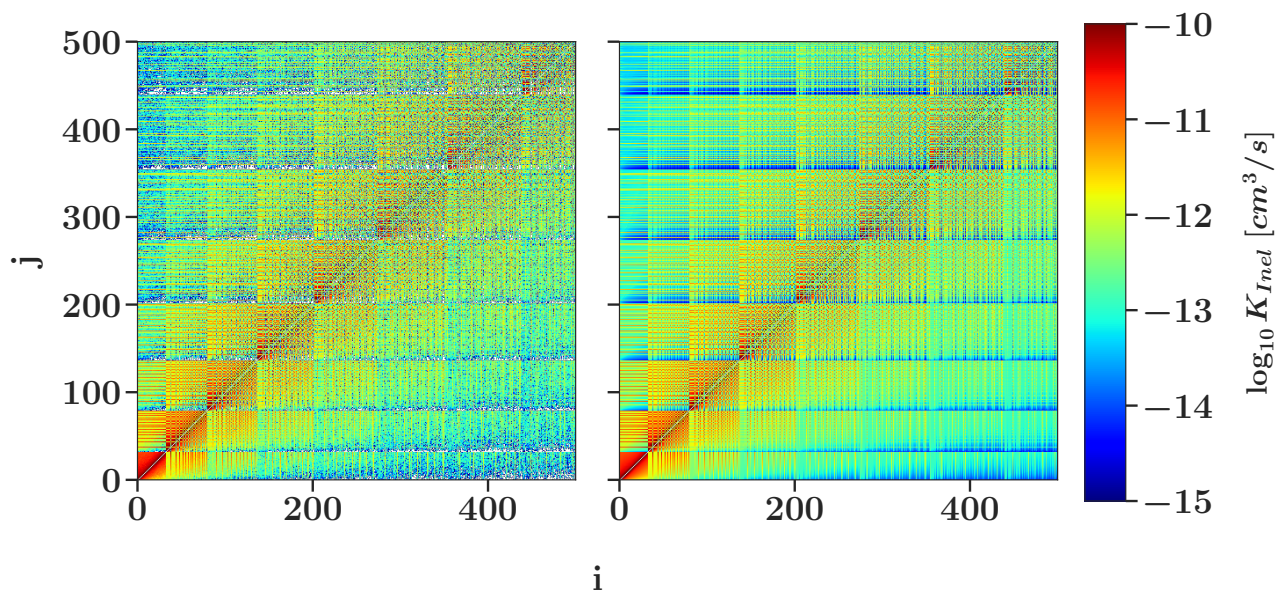(b)Zoomed-in StS Inelastic Rate Coefficient Matrix

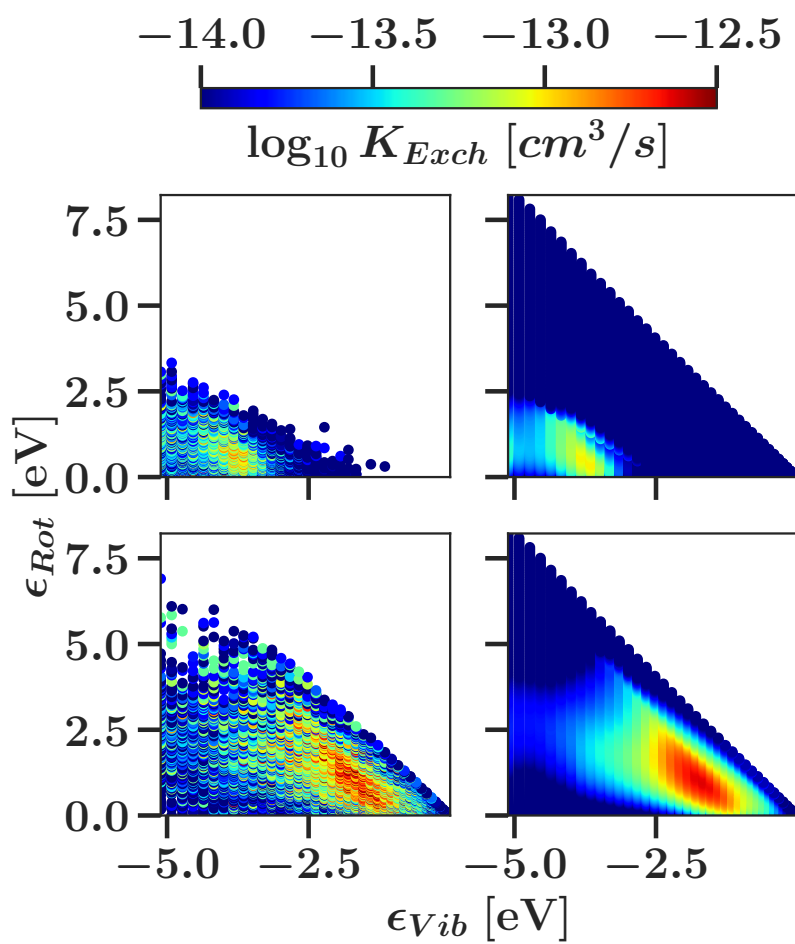**Figure S8:** Comparison between inelastic rate coefficients from QCT and SurQCT predictions at T = 2,500 K.
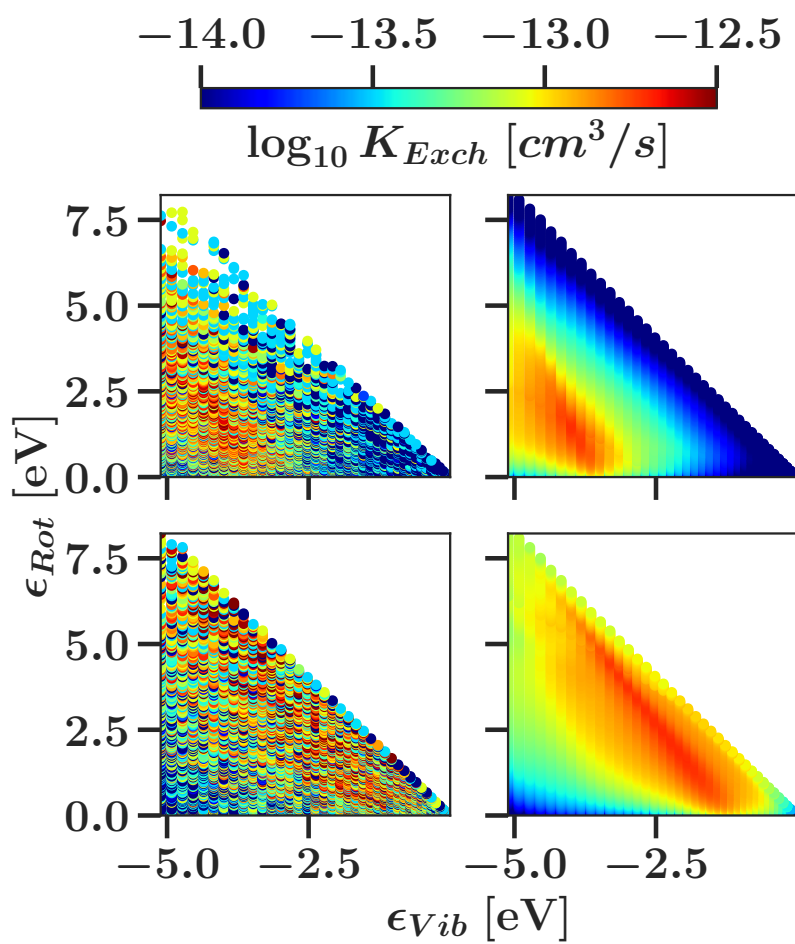
(a)Full StS Inelastic Rate Coefficient Matrix

(b)Zoomed-in StS Inelastic Rate Coefficient Matrix

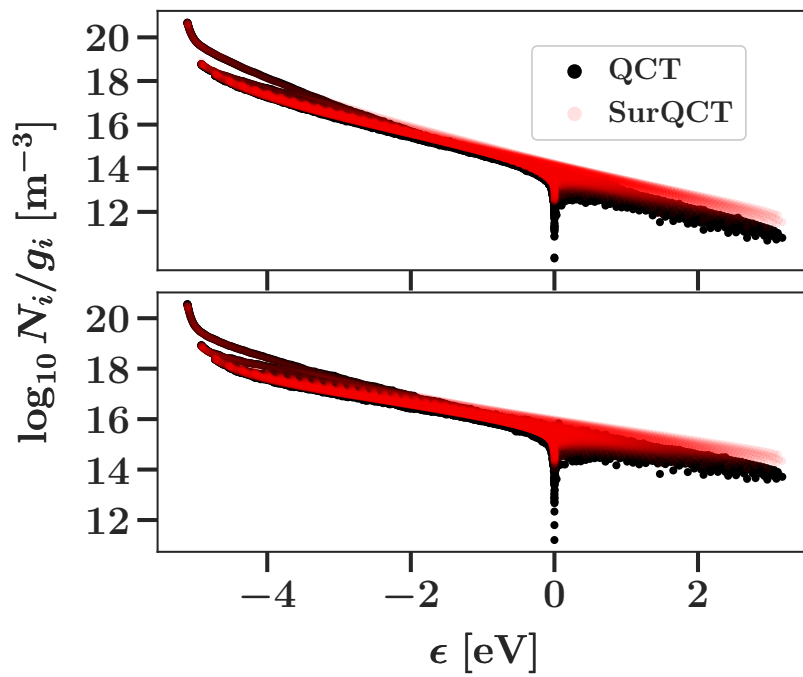**Figure S9:** Comparison between inelastic rate coefficients from QCT and SurQCT predictions at T = 20,000 K.

Figure S10: Comparison between exchange rate coefficients from QCT and SurQCT predictions at T = 2,500 K.

Figure S11: Comparison between exchange rate coefficients from QCT and SurQCT predictions at T = 20,000 K

VII.   NON-BOLTZMANN POPULATION DISTRIBUTION

Figure S12: Population distribution comparison between QCT-based solutions and SurQCT-based solutions at t = 1e-7s for T = 8,000 K (top) and t = 5e-8s for T = 20,000 K (bottom).

VIII. COMPARISON OF TRAINING A FEED-FORWARD NEURAL NETWORK

A feed-forward NN with the same optimization, activation functions and number of parameters as the DeepONet is trained for inelastic rate coefficients. This is done to demonstrate and justify the use of the DeepOnet architecture.

(a)

(b)
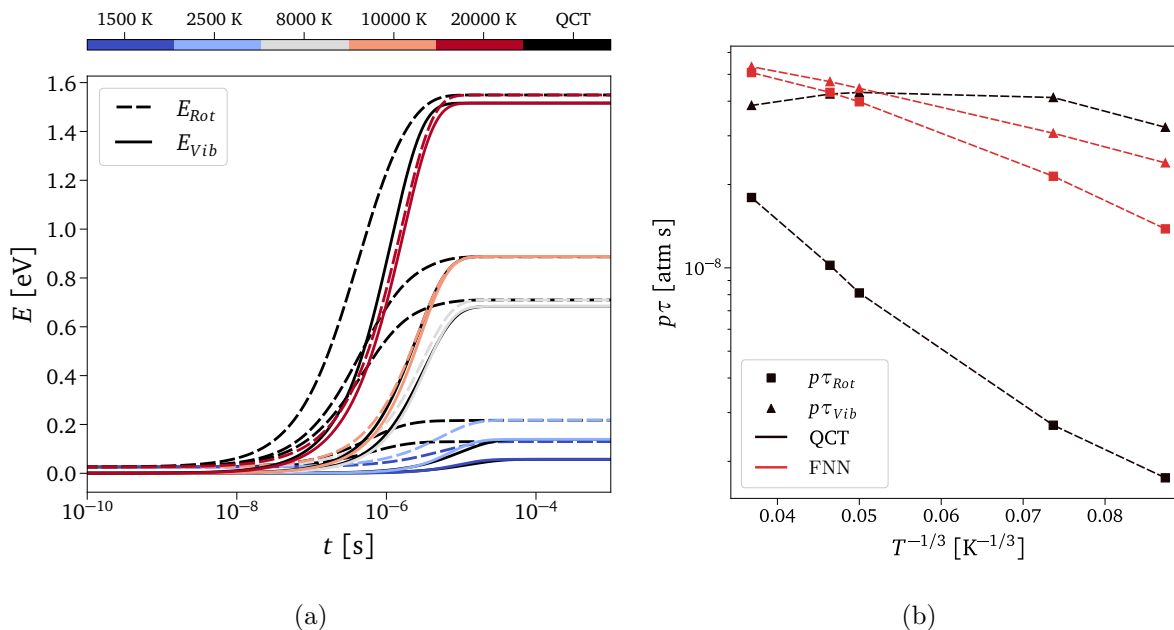
Figure S13: (a) Evolution of rotational and vibrational energies in isothermal heat bath simulations at different translational temperatures. The continuous lines refer to simulations that rely on complete QCT rate coefficient databases, while the dashed lines are obtained based on rate coefficients predicted by the trained FNN. (b) Comparison of rotation and vibration relaxation times.

Layers: [7-in,100,100,100,1-out]; Act. fun.: [tanh - tanh - tanh - linear]; Tot. parameters: 21,101

REFERENCES

[1]D. Koner, O. T. Unke, K. Boe, R. J. Bemish and M. Meuwly, *The Journal of Chemical Physics*, 2019, **150**, 211101.